

### 3D Thermal Imaging: Fusion of Thermography and Depth Cameras

by J. Rangel\*, S. Soldan\*\*, A. Kroll\*\*

\* University of Kassel, Faculty of Mechanical Engineering, Measurement and Control Department, Mönchebergstrasse 7, 34125 Kassel, Germany, [johannes.rangel@student.uni-kassel.de](mailto:johannes.rangel@student.uni-kassel.de)

\*\*Same Department, [{samuel.soldan, andreas.kroll}@mrt.uni-kassel.de](mailto:{samuel.soldan, andreas.kroll}@mrt.uni-kassel.de)

#### Abstract

This work presents an approach to automatically create 3D thermal models using multi-perspective measurements with a multimodal camera system consisting of a thermal camera and a depth camera. Additional attributes such as color can also be added to the model. The paper centers its attention on the geometrical calibration of the cameras and the validation of the results. The design of an adequate calibration target is discussed and different options are evaluated. To expose the applicability of the approach two inspection tasks are used as examples.

#### 1. Introduction

##### Motivation and Problem Statement

Thermal imaging has become a helpful and widely used tool for inspection and control tasks in industrial applications [1,2]. Since a single thermal image alone is often not sufficient in large and complex inspections tasks and self-explanatory (i.e. on sceneries where temperature gradients are small or when dealing with large objects), additional data like color photos, position and orientation of the camera, environment conditions, thermograms of the surrounding area due to limited FOV or close-ups are required for documentation and decision making. Visual images, for example, can be used for enhancing thermal image segmentation algorithms since visual images give a different representation of the scene (complementary information). Thermal imaging can also be used as complementary information where the main used modalities are from another nature (i.e. spatial or color data as main source of information). Taking this into account, the fusion of thermal and spatial information is considered in this work by using a thermal camera and a depth camera for obtaining 3D-thermal models (see **Figure 1**).

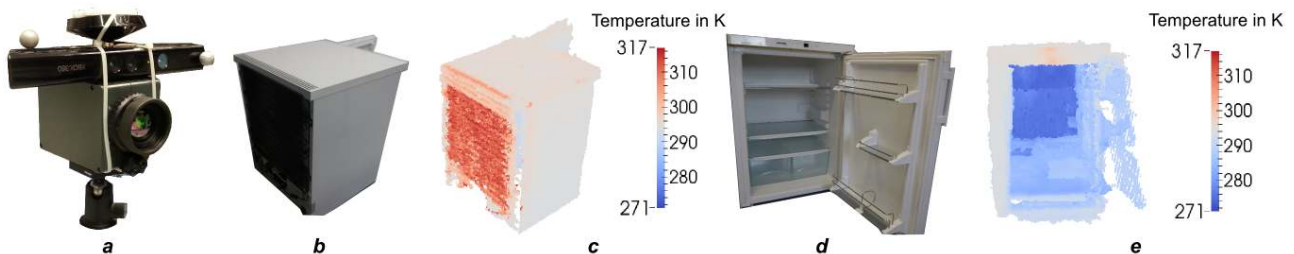


**Figure 1.** a: Multimodal system with a Jenoptik IR-TCM 640 thermography camera and Microsoft Kinect depth camera. b - e: 3D-thermal model of a fridge. Fridge (back) (b: color – c: thermal); Fridge (front) (d: color – e: thermal).

##### State of the Art

The fusion of thermal and spatial information has gained attention in the last years, especially in fields where the spatial data is used as main source of information (i.e. building modeling [3,4,5,6]). In some applications, the 3D-thermal models are built by using image-processing techniques [6,7]. In many other applications a multi-sensor system is used where at least one thermal camera is required as thermal information source. Spatial data can be obtained by means of different sensors, such as:

- Laser range finder [8,9]
- Depth camera [3,10]
- Visual camera [11,12]
- Second thermal camera [13]

All these multi-sensor systems have to be calibrated in order to know the spatial relation between the sensors. This can be carried out using a calibration target [10,14,15,16]. When the system is calibrated, a 3D thermal representation from the scene can be obtained. However, in the above-mentioned publications the design and suitability of the calibration target is not well-explained or considered at all. Different camera positions and orientations are also often not considered to create a complete 3D representation of the whole scene (not just limited by the FOV of the camera).

## 2. Thermal and Depth Information Fusion

### System Description

A stereo-multimodal system based on a thermal camera (Jenoptik IR-TCM 640, Focal length: 30 mm, FOV: 30°X23°, Spectrum: 7 μm - 14 μm, image size: 640x480) and a depth camera (Microsoft Kinect, Focal length: 6.1 mm, FOV: 57°X45°, image size: 640x480) was used in this application. The cameras were arranged in a way that their lenses were horizontally aligned (see **Figure 2** (left)). They were attached to each other using Velcro sheets and a damping band between the contact surfaces of the two cameras. Zip ties were also used to make the connection more rigid.



**Figure 2:** a: Stereo-multimodal system setup. b: Field of view (FOV) relationship between the cameras.

Because of the different field of views (FOVs) of the cameras (see **Figure 2** (right)), it is expected that the spatial data as well as the thermal data are not completely used.

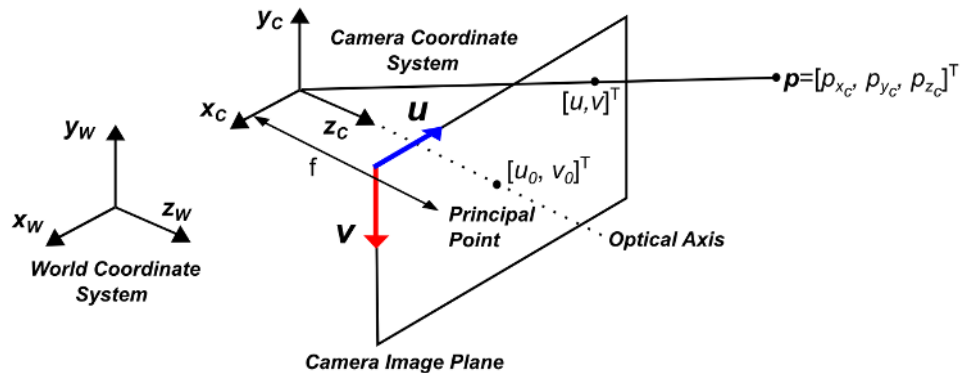


**Figure 3:** Pinhole Camera Model

### Geometric Model

For geometrically describing the system, first each camera was considered as a pinhole camera. In the pinhole camera model, the relation between the 3D world and the 2D image is described through a perspective projection [17,18]. An actual pinhole camera has no optical distortion, since the light travels in a straight light through the pinhole (see **Figure 3**). However, the path of light in a lens is quite complex because of the number of elements and the physical phenomena involved. The tangential and radial distortion of the camera can be modeled adding a special term to the pinhole-camera equations. The following pinhole camera based equations are widely accepted for describing camera projections:

$$\mathbf{p} = \begin{bmatrix} p_{x_c} \\ p_{y_c} \\ p_{z_c} \end{bmatrix} = \begin{bmatrix} m p_{z_c} \\ n p_{z_c} \\ p_{z_c} \end{bmatrix} \quad (1)$$

$$r^2 = m^2 + n^2 \quad (2)$$

$$\begin{bmatrix} s \\ t \\ 1 \end{bmatrix} = \text{dist} \left( \begin{bmatrix} m \\ n \\ 0 \end{bmatrix}, \mathbf{k} \right) = (1 + k_1 r^2 + k_2 r^4 + k_5 r^6) \begin{bmatrix} m \\ n \\ 0 \end{bmatrix} + \begin{bmatrix} 2k_3 m n + k_4 (r^2 + 2m^2) \\ 2k_4 m n + k_3 (r^2 + 2n^2) \\ 1 \end{bmatrix} \quad (3)$$

$$K = \begin{bmatrix} f_x & 0 & u_0 \\ 0 & f_y & v_0 \\ 0 & 0 & 1 \end{bmatrix} \quad (4)$$

$$\begin{bmatrix} u \\ v \\ 1 \end{bmatrix} = K \begin{bmatrix} s \\ t \\ 1 \end{bmatrix} \quad (5)$$

where  $\mathbf{p} = [p_{x_c}, p_{y_c}, p_{z_c}]^T$  is a 3D point in the camera coordinate system,  $[u, v]^T$  is a point in the image coordinate system,  $\mathbf{k} = [k_1, k_2, k_3, k_4, k_5]$  is a vector of the radial and tangential distortion parameters and  $K$  is a positive definite matrix called the camera matrix ( $[f_x, f_y]$ : focal length scaling factors,  $[u_0, v_0]$ : principal point).  $K$  and  $\mathbf{k}$  are called the camera intrinsic parameters. The variables  $r, m, n, s$  and  $t$  are intermediate variables that are used to simplify the representation of the equations. The spatial relation between the arranged/fixed cameras (normally horizontally aligned) of the system is represented by means of a 4x4 transformation matrix  $T$  composed by a 3x3 rotation matrix  $R$  and a 3x1 translation vector  $\mathbf{t}$ .

$$T = \begin{bmatrix} R & \mathbf{t} \\ 0 & 1 \end{bmatrix} \quad (5)$$

Using this transformation matrix, a 3D point  $\mathbf{p}$  in the coordinate system of one of the cameras can be transformed into the coordinate system of the other one. This means that pixels from one camera image can be mapped to another camera image since the depth (spatial) information of the scene is known. With the matrix  $T$  and the intrinsic parameters of both cameras a point  $[u_D, v_D]^T$  from the depth camera image can be mapped into the thermal image ( $[u_T, v_T]^T$ ) by using the following equations:

$$\mathbf{p}_D = d \text{ dist}^{-1} \left( K_D^{-1} \begin{bmatrix} u_D \\ v_D \\ 1 \end{bmatrix}, \mathbf{k}_D \right) \quad (6)$$

$$\begin{bmatrix} \mathbf{p}_T \\ 1 \end{bmatrix} = T \begin{bmatrix} \mathbf{p}_D \\ 1 \end{bmatrix} \quad (7)$$

$$\begin{bmatrix} u_t \\ v_t \\ 1 \end{bmatrix} = K_T \text{ dist} \left( \mathbf{p}_T \frac{1}{d}, \mathbf{k}_T \right) \quad (8)$$

where  $\mathbf{p}_D$  is a 3D point on the depth cameras coordinate system,  $d$  the depth information from the depth image,  $\text{dist}$  the distortion function described by equation (3),  $K_D$  the depth camera matrix,  $\mathbf{k}_D$  the distortion coefficients of the depth camera,  $\mathbf{p}_T$  a 3D point on thermal cameras coordinate system,  $K_T$  the thermal camera matrix and  $\mathbf{k}_T$  the distortion coefficients of the thermal camera.

### Geometric Camera Calibration

In order to find the intrinsic parameters of a camera it is necessary to carry out a calibration process (geometric calibration). In this work a widely accepted calibration method described in [19] was used. It requires a flat calibration target that contains several detectable markers in known positions (calibration pattern). Once the calibration pattern is detected in the images, a calibration algorithm is carried out relating the image coordinates and the spatial coordinates of the detected markers (features). Similarly, for finding the spatial relation between the two cameras one image it is required from each camera (simultaneously taken) of a common calibration target (stereo calibration). By means of an algorithm that uses the intrinsic parameters (obtained from the geometric calibration) of each camera for finding the position and rotation of the calibration target with regard to each camera the transformation matrix  $T$  (equation 5) is obtained. This means that the markers of the calibration target have to be suitable for both cameras. Taking this into account, different materials and calibration features were tested for designing a suitable target.

### 3. Calibration Target

As it was mentioned above, the geometric calibration of cameras and stereo camera systems is generally carried out using a flat calibration target. This target contains detectable features for the camera arranged in a known pattern. In a thermal camera, the information obtained from it is related to the reflected infrared (IR) rays of the objects in the scene. Materials with a high emissivity do not absorb much infrared energy so they reflect most of the IR-rays back. For that reason, calibration targets made of materials with different emissivities are suitable for thermal camera calibration (e.g. PCB (Printed Circuit Board).  $\epsilon_{FR4} = 0.99$ ,  $\epsilon_{gold\ plated} = 0.0575$ ). In [14,20,11], for example, aluminum was used due to its high emissivity. In [10] Styrofoam was used.

The Kinect obtains the spatial information of the scene based on an IR-light pattern detected by a near-IR camera. This means that the depth data as well as the near-IR data from the Kinect can be used for its geometric calibration. When dealing with depth images, calibration targets made of transparent materials [21] or with holes [10] are suitable because they create a depth change in the scene. For near near-IR images, since the near-IR spectrum is close to the visual spectrum, materials for calibration of normal cameras (e.g. paper [22]) can be used while illuminating them i.e. with a halogen lamp.

### Target Classification

Considering the overview in the literature, targets can be classified into different categories (see **Figure 4**). Based on its working principle, a target can be passive or active. Passive targets don't use external energy sources for being detectable by the sensor. They exploit the emissivity  $\epsilon$  of their material. Active targets use external energy sources to be detected (e.g. calibration targets with lightbulbs for thermal camera calibration). A target can be also classified based on the features (markers) it uses. Features represent gradient changes of pixel intensities in an image. These gradient changes can be obtained by using different kind of features (i.e. corners, circles, lines, rings, etc.). Depending on how the markers are arranged in the calibration target, a target can be structured or unstructured. Structured patterns have features arranged in known coordinates (e.g. symmetric/asymmetric grids) whereas features in unstructured pattern have unknown positions that have to be measured before any calibration. **Table 1** shows some examples of calibration targets with their respective classification.

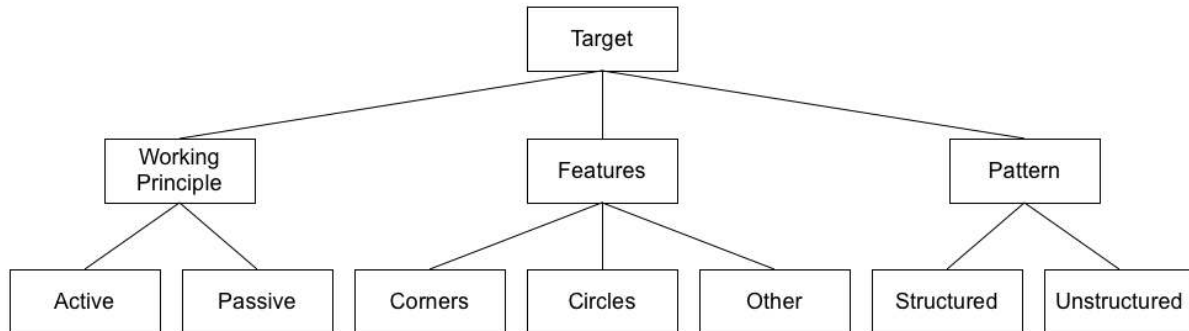


**Figure 4.** Calibration target classification

**Table 1.** Examples of calibration targets

Target type	Checkerboard [14]	Hermann grid [10]	Square grid [23,24]		Asymmetric grid	Unstructured [16]
Picture						
Working principle	Passive	Passive	Passive	Active	Passive	Passive
Features	Corners	Corners	Circles	Circles	Circles	Other
Pattern	Structured	Structured	Structured	Structured	Structured	Unstructured

### Manufacturing Considerations

One of the goals of designing a calibration target for this multimodal system is to have a suitable, easy to manufacture and not expensive target. Active targets require, in most of the cases, electrical devices (e.g. cables, lightbulbs, etc.) [12,23], which increases the complexity of the target. Such targets are also expensive and don't guarantee a good precision since they are in most of the cases handmade. For that reason, the design of a passive target was carried out considering the working principle of each camera (Thermal camera: IR, Kinect: near-IR structured light), the common characteristics between the modalities involved and the intrinsic parameters of the cameras (i.e. FOV for designing the size of the target). In order to find the most suitable material, feature, pattern and size, a set of tests was carried out using standard camera calibration software (OpenCV [25]) and varying the features, materials and patterns of the target.

### Tests of Features and Materials

Targets used for single thermal and single depth calibration were tested using the thermal, depth and near-IR modalities. Paper, PCB, glass and firm cardboard were used (**Figure 5**). Line intersections (corners) and circles as detectable markers (features) arranged in symmetric and asymmetric patterns were tested. **Figure 6** shows the results.



**Figure 5.** Various tested calibration targets. From left to right: Paper (chessboard), glass (chessboard), PCB (chessboard), laser-cut firm cardboard target (asymmetric circles).

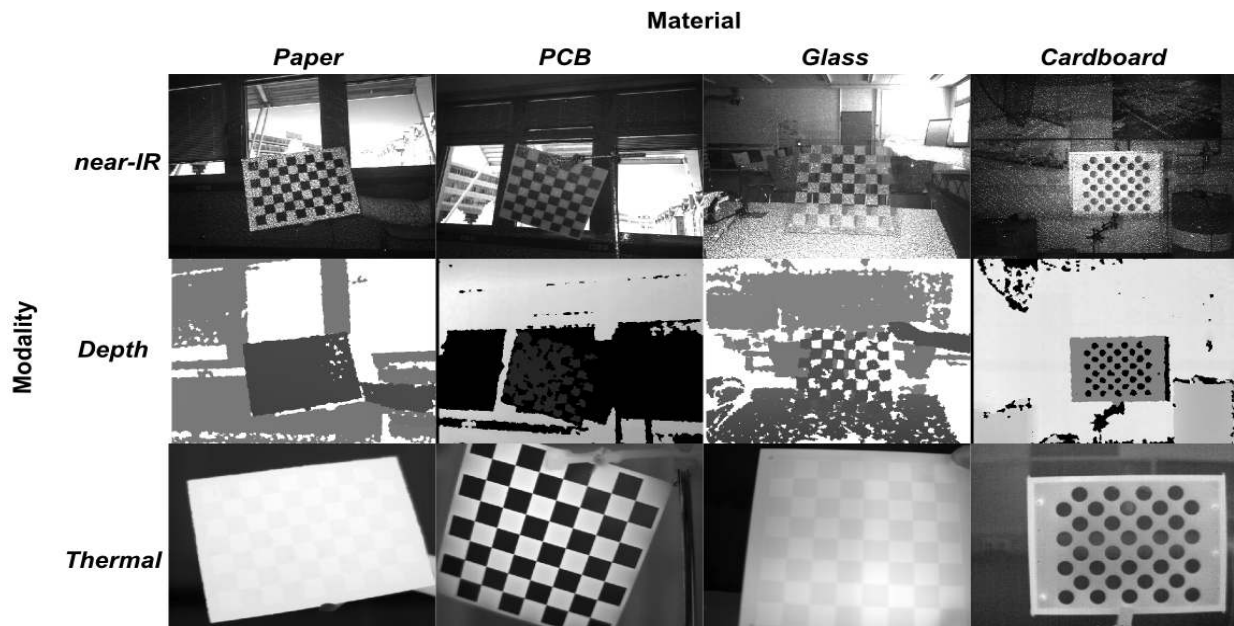


**Figure 6.** Images of different calibration targets depending on camera modality and target material

### Target Selection

As it can be observed in **Figure 6**, features are apparent for both cameras when the emissivity of the markers is different with regard to the target's surface. The quantity and position of the markers in the target depends on the target's size. Tests using the PCB checkerboard showed that this target could be used for the calibration of the multimodal system. However, special light conditions for the near-IR image of the depth camera have to be guaranteed and the target has to be big enough so the calibration pattern can be detected. This last condition implies higher manufacture costs that can be avoided by using other materials. In [26,27] it is shown that better calibration results can be obtained when having circles instead of corners as detectable features. Considering these observations cardboard and circular holes were chosen as material and features, respectively. The thermal/reflective properties of cardboard ( $\epsilon_{card} = 0.81$ ) are suitable for taking thermograms when its surface is heated, such that a temperature difference to the background is obtained. The circles (holes) are also detectable in the near-IR and depth image of the Kinect (see **Figure 7**).

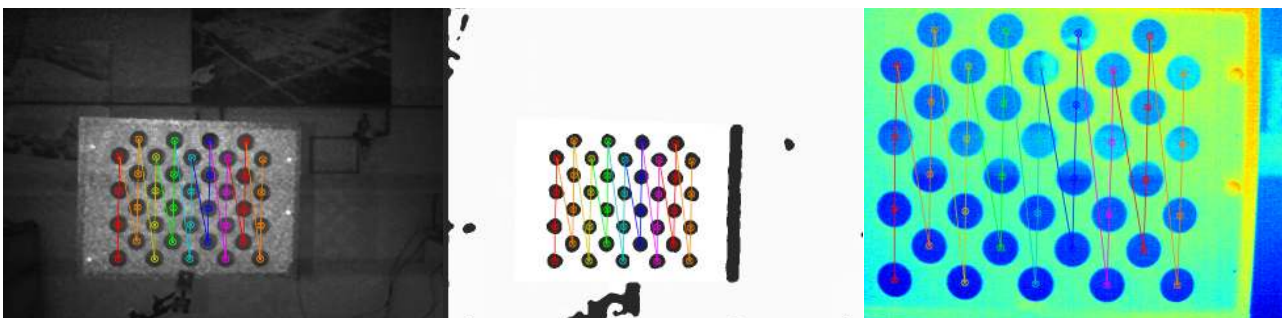


**Figure 7.** Calibration pattern recognized in each modality (near-IR (left), depth (middle), thermal (right))

## Target Dimensions

The target/calibration pattern size and the spatial range, where the target is positioned with respect to the cameras system, are obtained by considering the FOV of both cameras, the effective range of the depth camera and the focus of the thermographic camera. The number of pixels on an image that an object occupies in horizontal and vertical direction can be calculated using the following relations based on the geometry of the pinhole model:

$$h = f_x \frac{H}{z} \quad (9)$$

$$v = f_y \frac{V}{z} \quad (10)$$

$$f_x = f \cdot s_x \quad (11)$$

$$f_y = f \cdot s_y \quad (12)$$

$$s_x = \frac{n_x}{2f \tan\left(\frac{FOV_h}{2}\right)} \quad (13)$$

$$s_y = \frac{n_y}{2f \tan\left(\frac{FOV_v}{2}\right)} \quad (14)$$

where  $h$  and  $v$  are the objects width and height, respectively, in pixels,  $H$  and  $V$  are the objects width and height in the real world,  $z$  is the distance of the object to the camera,  $f_x$  and  $f_y$  are the focal length scaling factors in horizontal and vertical direction,  $f$  the focal length,  $s_x$  and  $s_y$  the scaling factors,  $FOV_h$  and  $FOV_v$  the angle of view in horizontal and vertical direction, respectively,  $n_x$  and  $n_y$  are the dimensions (in pixels) of the image in horizontal and vertical direction. Considering that the calibration target uses circles (holes) as features, the diameter of the holes can be calculated using the following equation:

$$d_h = \frac{n_x z}{f_x c} \quad (15)$$

where  $c$  is the number of holes on the target in the horizontal direction (columns). The number of rows  $r$  (number of holes in the vertical directions) can then be obtained using:

$$r = \frac{n_y z}{f_y d_h} \quad (16)$$

Taking the parameters of the thermal camera (image size: 640x480), a minimal distance  $z$  between system and calibration target of 1 m (the effective range of the depth camera is 0.8-3.5 m [22]) and choosing a number of columns  $c = 9$  of the pattern, a hole diameter  $d_h = 50$  mm and a number of rows  $r = 8$  are inferred. This carries to a targets size of 60x45 cm. Using  $z$  as parameter, a fixed focus of the thermal camera was set.

## 4. Geometric Calibration of the System

The geometric calibration of the multimodal system is carried out in two steps. First, a single geometric calibration is performed for each camera for finding the respectively intrinsic parameters. The geometric calibration of the thermal camera was carried out using the designed calibration target. The target was heated up with a dryer in order to get images with a better contrast. The depth camera was calibrated using the same target and the near-IR images. 20 images were taken for each camera. The calibration algorithm detects the features in each image, estimates the initial calibration parameters (without considering the distortion parameters) by a closed-form solution and then optimizes them by Levenberg-Marquardt (including distortion parameters) to minimize the reprojection error. For the stereo calibration of the system at least one image of the designed calibration target from each camera is required. Using the intrinsic parameters of the cameras the position and orientation of the calibration target with respect to each camera's coordinate system is obtained and so is the spatial relation between them. Knowing the spatial relation between the cameras, depth information can be remapped to thermal information by using equation (8).

### Parallax Effect Correction

Depending on the scene, there may be some points that are seen by only one camera (see **Figure 8**). This means that for two reprojected points from the depth camera a single temperature value (point  $v_p$  in **Figure 8**) is going to be assigned. This is called the parallax effect. Considering that the lenses of the camera are horizontally aligned the reprojected images can be corrected by filtering duplicated image coordinates in vertical direction.



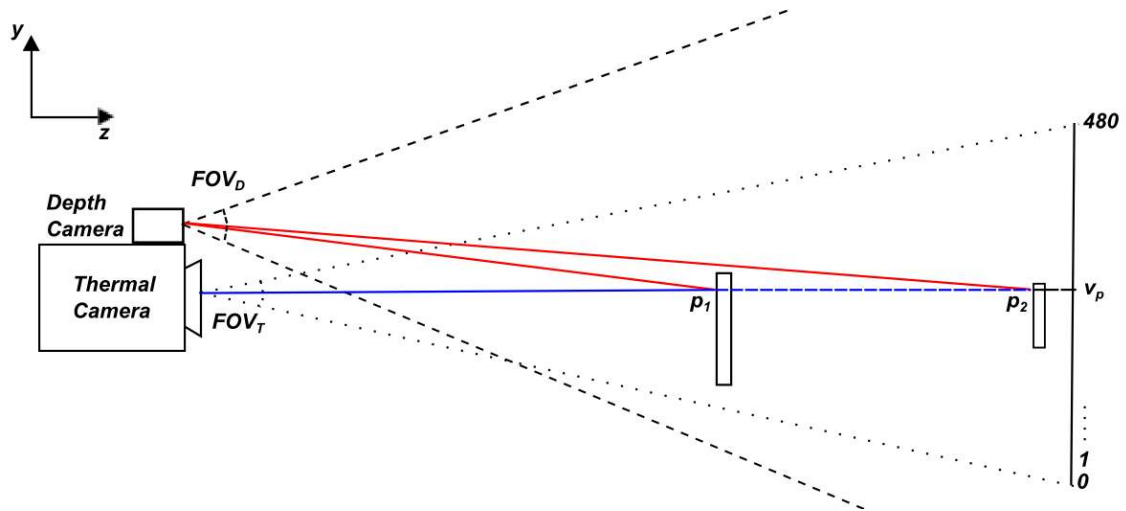


Figure 8. Parallax effect.

## 5. Validation

In order to validate the results of the single and stereo calibration of the cameras three approaches are used: Visual analysis, mean reprojection error of a set of reprojected points and by using a motion tracking system (MTS).

### Visual Analysis

The simplest approach to find out if the fusion of the data was performed in a good way is by looking at the reprojected images using the calibration board. As it can be seen in **Figure 9** the fusion between the depth image and the thermal image is carried out correctly.

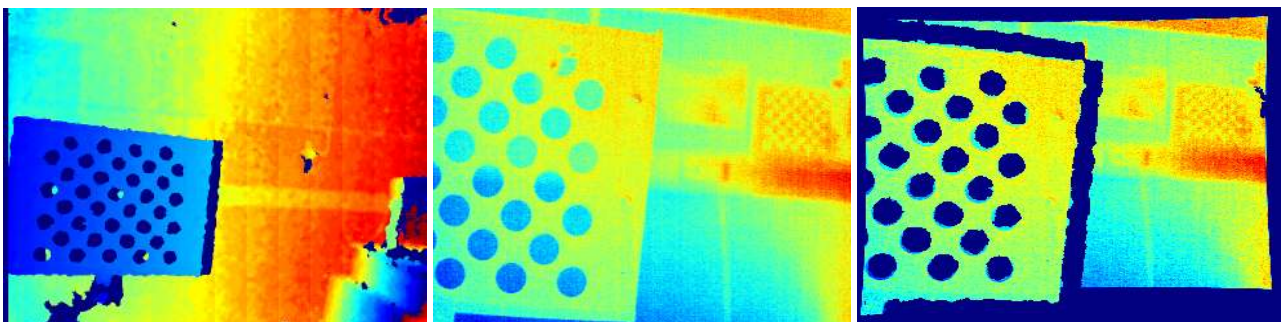


Figure 9. Visual validation of the thermal-depth fusion. Depth image (left). Thermal image (middle). Fused image (right).

### Mean Reprojection Error

The accuracy of the fusion can be analyzed by looking at the reprojection error, which represents the distance (error) between a detected point and a reprojected point in an image. 20 images of the calibration board were taken for this purpose. Since 36 markers can be detected in each image of the calibration target, a total of 720 points were used to test the accuracy of the calibration. Each detected point from the near-IR image was reprojected to the thermal image using the equations (6), (7) and (8) and then compared to the respective detected point on the thermal image, so a reprojection error can be calculated. A mean reprojection error (from the 720 points) of about 0.5 pixels (about 1.3 mm in space) was achieved.

### Validation using a MTS

A motion tracking system (MTS) gives the position of objects within a workspace when markers are placed on them. Using a MTS a reprojection error of the multimodal fusion can be measured, since a point with known position in the MTS can be reprojected to each camera's image. The first step is to calibrate the multimodal system with respect to the MTS. This can be achieved by using the designed calibration target. Markers were placed on both the multimodal

system and the calibration target so their position with regard to the MTS coordinate system is known. Taking an image of the calibration target (see **Figure 10** left) the transformations  $T$  and  $T_{MD}$  (see **Figure 10** right) are obtained.

Not changing the position of the multimodal system ( $T_{MD}$  is constant) and changing the position of the calibration target the position of a point  $p$  (see **Figure 10** right) in the calibration target with regard to the MTS coordinate system ( $T_{Mp}$ ) can be transformed to each camera's coordinate system and projected to each camera's image. Comparing the projected and detected points in the image an error can be calculated. After testing different positions it was noticed that the spatial error is about 1,5 mm.

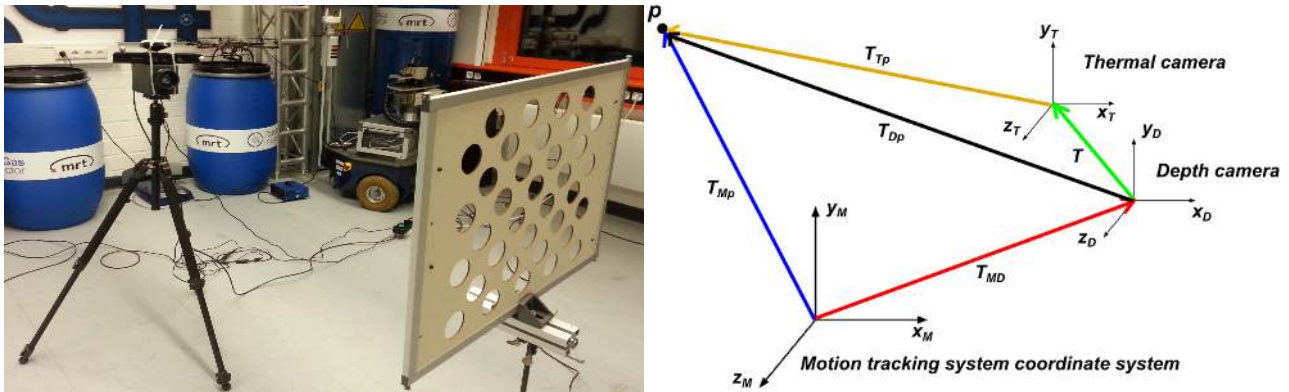


**Figure 10.** Calibration setup (left). Coordinate system arrangement: multimodal system and MTS (right).

## Discussion

The mentioned approaches have shown to be effective for analyzing and validating the results of the thermal/spatial data fusion. The visual analysis has demonstrated that the mapping between thermal and depth images and the parallax effect correction have been done correctly. However, it is not possible to determine the accuracy of the mapping with this approach since no benchmark is used. By using the mean reprojection error of a set of reprojected points, a measure of how accurate the system is, can be obtained. The results have shown a mean reprojection error smaller than one pixel. When using a MTS for validating the results, a mean reprojection error can be obtained as well. Results have shown that the obtained mean reprojection errors from the last two approaches correspond to each other. Sources of error like varying the focus settings of the thermal camera and the calibration of the MTS were considered for detecting and correcting systematic errors.

## 6. Application: 3D Thermal extended Data

Using a motion tracking system, multiple measurements (scenes) can be matched and a more complete representation of objects or rooms can be obtained. For this purpose, the multimodal system and the MTS have to be calibrated in the same way described above. It is also necessary that the workspace of the MTS is big enough to enable free movements of the multimodal system. By moving the multimodal system around an object or a room data from different perspectives as well as the camera's position and orientation are obtained and saved. These data can be matched spatially by a transformation to the global MTS coordinate system. With help of a point cloud visualization software, information of interest (e.g. spatial, visual and thermal) can be filtered in order to obtain the desired representation. **Figure 11** and **Figure 12** show 3D-thermal representations of an outstretched utility corridor, which has been obtained using the process mentioned above.

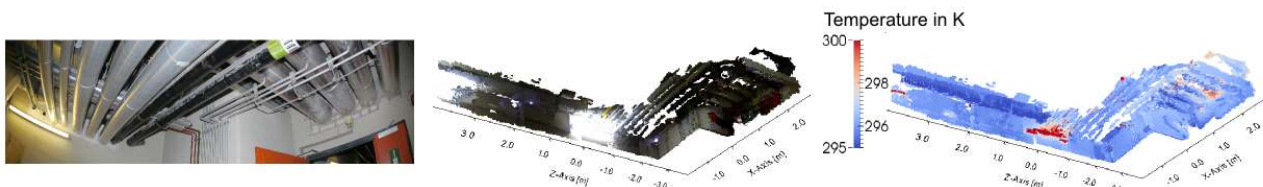


**Figure 11.** 3D-representation of a utility corridor 1. Left: Picture of the place. Middle: Visual-3D representation. Right: Thermal-3D representation.





**Figure 12.** Second 3D-representation of a utility corridor 2. Left: Picture of the place. Middle: Visual-3D representation. Right: Thermal-3D representation.

## 7. Summary and Outlook

In this work a multimodal system based on a thermographic camera and a depth camera was used for fusing thermal and spatial data. Two cameras were arranged in a fixed way and their spatial relation was obtained by means of a geometric calibration (which requires a calibration target) based on the pinhole camera model. The design and nature of the calibration target determines the success of the calibration and depends on the working principle of the cameras and manufacturing precision. The calibration success was assessed by inspecting the image visually, by measuring the reprojection error between markers (features) that are detectable on both images and by using a motion tracking system, which delivers accurate positions of objects with regard to a global coordinate system. Results showed that the reprojection error is smaller than one pixel. Together with the motion tracking system, measurements from different perspectives of a scene were taken. Knowing the position and orientation of the multimodal system with respect to the motion tracking system, all measured data can be transformed and matched into a common coordinate system. From this, a complete representation is obtained, where thermal, visual and depth information can be selected. The distance to the objects and their emissivity have to be taken into account for obtaining better results. Next works will address alternative sensors for obtaining depth information from the scene (e.g. laser range finder, visual camera, another thermal camera). 3D data processing techniques for enhancing the obtained 3D models as well as feature extraction and segmentation algorithms for finding information of interest within the obtained data are going to be considered.

## REFERENCES

- [1] M. Vollmer and K. P. Möllmann, *Infrared Thermal Imaging*. Weinheim: Wiley VCH, 2010.
- [2] H. Kaplan, *Practical Applications of Infrared Thermal Sensing and Imaging Equipment*. Bellingham: SPIE, 2007.
- [3] S. Vidas, P. Moghadam, and M. Bosse, "3D thermal mapping of building interiors using an RGB-D and thermal camera," in *Robotics and Automation (ICRA), 2013 IEEE International Conference on*, pp. 2311-2318.
- [4] Y. Ham and M. Golparvar-Fard, "Rapid 3D energy performance modeling of existing buildings using thermal and digital imagery," in *Construction Research Congress 2012*, West Lafayette, Indiana, United States, 2012, pp. 991-1000.
- [5] S. Lagüela, L. Díaz-Vilariño, J. Armesto, P. Arias, and C. L. M. Vigo, "Thermographic 3D models as the foundation for Building Information Models.," in *11th International Conference on Quantitative InfraRed Thermography*, paper QIRT-2012-180, Naples, Italy, 2012.
- [6] D. Iwaszczuk, L. Hoegner, and U. Stilla, "Matching of 3D building models with IR images for texture extraction," in *Urban Remote Sensing Event (JURSE)*, Munich, Germany, 2011, pp. 25-28.
- [7] D. González-Aguilera, P. Rodríguez-González, J. Armesto, and S. Lagüela, "Novel approach to 3D thermography and energy efficiency evaluation," *Energy and Buildings*, vol. 54, pp. 436-443, November 2012.
- [8] K. Nagatani, K. Otake, and K. Yoshida, "Three-dimensional thermography mapping for mobile rescue robots," in *Field and Service Robotics.*: Springer Berlin Heidelberg, 2014, vol. 92, pp. 49-63.
- [9] D. Borrmann, H. Afzal, J. Elseberg, and A. Nüchter, "Mutual calibration for 3D thermal mapping," in *Proc., 10th Int. IFAC Symp. on Robot Control (SYROCO'12)*, vol. 10, Dubrovnik, Croatia, 2012.
- [10] K. Skala, T. Lipič, I. Sović, L. Gjenero, and I. Grubišić, "4D thermal imaging system for medical applications," *Periodicum biologorum*, vol. 113, no. 4, pp. 407-416, 2011.
- [11] P. Aksenok, I. Clark, D. Grant, A. Inman, L. Vartikovski and J.C. Nebel, "3D thermography for quantification of heat generation resulting from inflammation," in *Proceedings of the 8th 3D modelling symposium*, Paris, France, 2003.
- [12] R. Yang, W. Yang, Y. Chen, and X. Wu, "Geometric calibration of IR camera using trinocular vision," *Lightwave Technology*, vol. 29, no. 24, pp. 3797-3803, 2011.

- [13] P. Y. Lee, "3D mapping of surface temperature using thermal stereo," in *9th International Conference on Control, Automation, Robotics and Vision*, Singapore, 2006, pp. 1-4.
- [14] D. Rzeszutarski and B. Więcek, "An integrated thermal and visual camera system for 3D reconstruction," in *11th International Conference on Quantitative InfraRed Thermography*, paper QIRT-2012-238, Naples, Italy, 2012.
- [15] S. Soldan, J. Rangel, and A. Kroll, "An Overview of Calibration Boards for the Geometric Calibration of Thermal Cameras," in *InfraR&D 2011*, Hannover, Germany, 2011.
- [16] T. Luhmann, J. Piechel, and T. Roelfs, "Geometric calibration of thermographic cameras," *Thermal Infrared Remote Sensing*, vol. 17, pp. 27-42, 2013.
- [17] O. Faugeras and Q. T. Luong, *The Geometry of Multiple Images*. Cambridge, Massachusetts: MIT Press, 2001.
- [18] R. Hartley and A. Zisserman, *Multiple View Geometry*. Cambridge, UK: Cambridge University Press, 2010.
- [19] Z. Zhang, "A flexible new technique for camera calibration," *IEEE Transactions on Pattern Analysis and Machine Intelligence*, vol. 22, no. 11, pp. 1330-1334, 2000.
- [20] L. Acampora, L. De Filippis, F. Martucci, and A. Sorigi, "3D Reconstruction of Thermal Images," in *Proceedings of 26th Aerospace Testing Seminar*, Los Angeles (USA), 2011, pp. 263-277.
- [21] O. Kreylo. (2014, March) Doc-Ok.org. A developer's perspective on immersive 3D computer graphics. [Online]. <http://doc-ok.org/?p=313>
- [22] J. Smisek, M. Jancosek, and T. Pajdla, "3D with Kinect," in *Computer Vision Workshops (ICCV Workshops)*, Barcelona, Spain, 2011, pp. 1154-1160.
- [23] S. Lagüela, J. Martínez, J. Armesto, and P. Arias, "Energy efficiency studies through 3D laser scanning and thermographic technologies," *Energy and Buildings*, vol. 43, no. 6, pp. 1216-1221, 2011.
- [24] G. Cardone, A. Ianiro, G. Dello Iorio, and A. Passaro, "Temperature maps measurements on 3D surfaces with infrared thermography," *Experiments in fluids*, vol. 52, no. 2, pp. 375-385.
- [25] G. Bradski and A. Kaehler, *Learning OpenCV: Computer vision with the OpenCV library*.: O'Reilly Media, Inc., 2008.
- [26] A. Datta, J. Kim, and T. Kanade, "Accurate Camera Calibration using Iterative Refinement of Control Points," in *Workshop on Visual Surveillance (VS)*, Kyoto, Japan, 2009, pp. 1201 - 1208.
- [27] (2014, March) Software Package for Precise Camera Calibration. [Online]. [https://www.ri.cmu.edu/research\\_project\\_detail.html?project\\_id=617&menu\\_id=261](https://www.ri.cmu.edu/research_project_detail.html?project_id=617&menu_id=261)